Prediction of Aerodynamic Tonal Noise from Open Rotors

Anupam Sharma[a,*], Hsuan-nien Chen[b]

[a] *2341 Howe Hall, Department of Aerospace Engineering, Iowa State University, Ames, IA, 50011, USA*
[b] *K1 2C-35, Aerodynamics & Aeroacoustics Laboratory - Niskayuna, General Electric Global Research Center, One Research Circle, Niskayuna, NY, 12309, USA*

Abstract

A numerical approach for predicting tonal aerodynamic noise from "open rotors" is presented. "Open rotor" refers to an engine architecture with a pair of counter-rotating propellers. Typical noise spectra from an open rotor consist of dominant tones, which arise due both to the steady loading/thickness and the aerodynamic interaction between the two bladerows. The proposed prediction approach utilizes Reynolds Averaged Navier Stokes (RANS) Computational Fluid Dynamics (CFD) simulations to obtain near-field description of the noise sources. The near-to-far-field propagation is then carried out by solving the Ffowcs Williams-Hawkings equation. Since the interest of this paper is limited to tone noise, a linearized, frequency domain approach is adopted to solve the wake/vortex-blade interaction problem.

This paper focuses primarily on the speed scaling of the aerodynamic tonal noise from open rotors. Even though there is no theoretical mode cut-

*Corresponding author
Email address: `sharma@iastate.edu` (Anupam Sharma)

off due to the absence of nacelle in open rotors, the far-field noise is a strong function of the azimuthal mode order. While the steady loading/thickness noise has circumferential modes of high order, due to the relatively large number of blades ($\approx 10 - 12$), the interaction noise typically has modes of small orders. The high mode orders have very low radiation efficiency and exhibit very strong scaling with Mach number, while the low mode orders show a relatively weaker scaling. The prediction approach is able to capture the speed scaling (observed in experiment) of the overall aerodynamic noise very well.

Keywords: open rotor noise, rotor-rotor interaction, CROR noise

1. Introduction

Single rotation propellers are highly efficient but are restricted to low forward flight speeds and are also limited in the thrust they can generate. A counter-rotating propeller design provides higher thrust and high aerodynamic efficiency at high flight speeds. This is possible because the aft, counter-rotating bladerow takes out the swirl put in by the front rotor. The fuel burn benefit over conventional, ducted fan designs is estimated to be more than 10 percent. A counter-rotating pusher propeller configuration is considered in this report and will henceforth be referred to as "open rotor" (see Fig. 1).

One of the technology roadblocks for the open rotor architecture is the associated aerodynamic noise. The noise spectra from an open rotor appear overwhelmingly tonal however the broadband noise contributes significantly to the overall EPNL (effective perceived noise levels) [1]. The tonal noise is

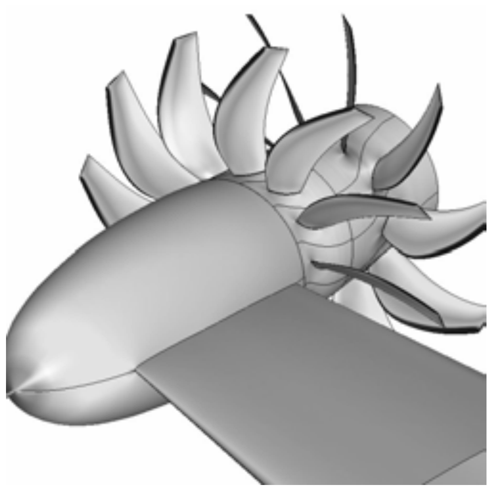

Figure 1: Open rotor configuration considered here for noise assessment.

caused by the aerodynamic and aeroacoustic interaction between the rotors, and the interaction between the rotors and the pylon/wing/fuselage. The same interactions also produce broadband noise due to the turbulence in the flow.

A methodology for numerical prediction of open rotor aerodynamic tone noise is presented here. The approach employs three-dimensional, RANS (for steady loading and thickness noise) and time-linearized RANS (for interaction noise) simulations to characterize noise sources in the near field. Such an approach has previously been successfully used to predict tone noise from fan-OGV interaction in a ducted configuration [2, 3, 4]. For an open rotor, an additional step of near-to-far field radiation is required, which is carried out by solving the Ffowcs Williams-Hawkings (FW-H) equation [5, 6] using the near-field sources defined on a translating, permeable surface. General Electric Company's proprietary flow solver, TACOMA [2, 7, 8] is used to carry out all the flow solutions used in the present work. A separate, frequency domain, FW-H solver has been developed which has been validated (results in following sections) against analytical solutions of canonical problems.

The concept of counter-rotating, un-ducted propellers was seriously investigated first in the early 1980s when oil price was soaring. Significant advances leading to engine flight tests were performed, but the ensuing slump in oil price put the concept on hold. In the last 5-8 years, the concept has been revived and is under serious consideration to be the choice propulsor for the next single-aisle aircraft. Since the concept of an open rotor has been around for a while, and aerodynamic noise has been one of its biggest design challenges, there is a rich history of publications in this field.

Peake and Parry [9] nicely summarizes the turbomachinery noise challenges facing modern turbofan engines with a focus on open rotors. The paper also provides a brief summary of the historic and recent progress in predicting and reducing open rotor noise. Hubbard [10] was the first to lay the foundations of counter-rotation propeller noise theory, which Hanson [11, 12] elaborated on and developed formulae for analytically predicting noise due to aerodynamic interference (wake interaction) between the two bladerows of a counter-rotating propeller. Hanson [11] also investigated the phenomenon of acoustic interference between the two rotors and between multiple modes from the same rotor. Several efforts have been devoted also into investigating the effects of angle of attack and the substantial noise increase observed when these machines are operated in non-uniform flow, see e.g., Mani [13] and Hanson [14].

Among recent efforts, Carazo *et al.* [15] demonstrated an analytical method for predicting tonal noise from open rotors, wherein the unsteady loading on the aft bladerow due to wake interaction is computed using Amiet's theory. Noise due only to dipole sources was considered and a far-field radiation model was derived from the formulation of a rotating acoustic dipole embedded in a uniform meanflow. Blandeau and Joseph [16] have further demonstrated an analytical capability to predict broadband noise in open rotors due to wake interaction between bladerows. The turbulence in the wakes is assumed to be homogeneous and isotropic in their analyses.

In recent years, considerable effort has gone into using the 3-D, Unsteady Reynolds Averaged Navier Stokes (U-RANS) approach for noise prediction, see e.g., Spalart [17] and Peters and Spakovszky [18]. Deconinck *et al.* [19] use the nonlinear harmonic approach to predict aerodynamic tonal noise from open rotors. They write the flow solution as a combination of the mean (time-steady) flow and the perturbation (time-unsteady) quantities. The perturbation quantities are represented as complex harmonics for frequencies of interest and solved for in the frequency domain. Significant time savings are achieved by realizing that only a few relevant frequencies are of interest and that for each frequency only a single passage simulation has to be carried out.

A recent three-part paper by Colin *et al.* [20, 21, 22] provides a comprehensive overview of various methods that can be used for open rotor noise evaluation. Their own numerical approach is also based on solving the U-RANS equations. They utilize the chorochronic approach wherein only a single passage of each bladerow is simulated, however time accurate data (of the order of periodicity in the blade row) needs to be accrued in the boundary cells. While theoretically, such direct simulation approaches should resolve all necessary physics of noise generation mechanisms, they all face the challenge of simultaneously resolving both the meanflow hydrodynamic scales and the small acoustic amplitudes. The linearized RANS approach utilized in the current paper isolates the acoustic problem by linearizing about the meanflow and hence permits accurate resolution of acoustics. For tone noise calculations, it is also very cost effective.

Parry *et al.* [1] investigated the relative importance of tonal versus broadband noise from "isolated" open rotors at zero angle of attack (similar configuration as considered here) and concluded that although there are a plethora of tones with significant protrusion above broadband noise, on a one-third octave level, the broadband noise cannot be ignored. While it is evidently important, no attempt is made here to predict broadband noise. In later sections, comparisons are drawn between measurements and prediction; the test data is decomposed into tonal and broadband components in a manner similar to that described in Parry [1].

Shielding of aerodynamic noise is one way to mitigate the noise challenge posed by the open rotor architecture. Towards this, Stephens and Envia [23] reported the experimental findings of an acoustic shielding experiment carried out in the 9" x 15" low-speed wind tunnel (LSWT) at NASA Glenn. They tested acoustic shielding from two (long and short) plates that are representative of an airplane wing or a horizontal/vertical stabilizer. They [23] also mention that the spatial resolution of the microphones is not enough to accurately resolve tonal noise directivity, as it can be very peaky. Installation effects on scattering of noise have also been investigated analytically - scattering by the aircraft fuselage treated as a hard infinitely long cylinder in [24] and scattering by the centerbody in [25].

The present paper focuses on a time-linearized, RANS-based numerical approach for open rotor tone noise prediction. While the methodology applies to any flight condition, the validation effort and focus is directed towards community noise at take-off condition. The following section describes the prediction process followed by validation against analytical solutions and comparisons against experimental data.

2. Prediction Process

The proposed open rotor aerodynamic noise prediction process involves multiple steps, which are summarized below. A flowchart illustrating the process flow is also provided in Fig. 2.

1. Multi-stage, RANS calculations are performed using TACOMA [7, 8] to compute meanflow solutions. One passage of each bladerow is simulated with periodic boundary conditions across passage boundaries (see Fig. 3). For each rotor, the simulation is performed in its frame of reference enabling steady state simulation for meanflow calculation. For validation cases, where measured aerodynamic performance data is available, the blade pitch is iteratively changed in CFD until shaft horse power (SHP) between the CFD and data are matched. This was required since the use of measured (when the blades were not running) pitch angles resulted in differences in predicted versus measured SHP of about a fraction of a percent. These differences can arise due to two reasons: (1) flexing of blades under aerodynamic and centrifugal loads, thus changing the blade pitch/twist during operation, and (2) errors in

the CFD method used in predicting aerodynamic loads (hence power). The shaft power differences can also be minimized by adjusting the shaft rotation speed in the simulations. However, changing the rotation speed will dramatically alter the radiation efficiencies of the tones (modes) and hence the predicted acoustic power in the farfield. Therefore, the choice of scaling by using pitch rather than rotor speed is preferable and is employed here.

2. Rotor alone noise sources (that due to blade thickness and steady loading) are obtained directly from RANS simulations described in step 1. Primitive flow variables are extracted on surfaces if front of, above, and aft of the simulated blade, which are then replicated (as many times as the number of blades) to form a full annulus surface enclosing all the blades of a rotor (see Fig. 4). This is the FW-H surface over which a boundary integral is evaluated for far-field noise prediction. Such a surface is also referred to as "permeable" surface as it allows flow through it. One of the benefits of using such a surface is that it only translates with the engine hence making the FW-H surface solver simpler; a surface on or around the individual blades (that rotates with the blades) will accelerate because of rotation. Time history for rotor alone (steady in rotor frame) field is obtained simply by rotating the flow variables on the FW-H surface with the shaft rotation rate. This is achieved cheaply by using uniform grid distribution in the circumferential direction and using the CSHIFT routine in Fortran 90.

3. For rotor-rotor interaction noise, an additional RANS simulation is carried out in the gap region between the two bladerows. This is performed

on a wake-tracking grid, to allow better resolution of the velocity gradients in the wake and hence minimize numerical errors. This procedure has previously been demonstrated by the authors [26] for ducted fans. From this solution, the front rotor wake is extracted at the inlet boundary of the CFD domain of the aft rotor and decomposed into front rotor blade passing frequency harmonics. Frequency domain, linearized unsteady Navier-Stokes analyses are then carried out independently for each harmonic. Only a single passage of the aft bladerow has to be simulated by applying the phase lag condition on the domain boundaries in the circumferential direction. Each rotor wake harmonic scatters into multiple frequencies (frequency scattering) as it interacts with the spinning aft rotor and produces what are often referred to as "sum" and "difference" tones. Unsteady primitive flow variables are extracted from the single-passage unsteady calculations and processed (using the phase lag boundary condition) to generate data on the full-annulus FW-H surface. The FW-H solver uses time-accurate, primitive flow variables on the permeable surface as input. The frequency domain solution is thus converted to the time domain by performing an inverse Fourier transform.

4. The last step involves solving the FW-H equation using time-dependent flow information on the FW-H surface. This step is the same for rotor alone and interaction noise prediction. Radiated sound power level can be obtained by integrating the sound intensity flux through a sphere surrounding the open rotor (sound source). The microphones in the experiments used for validation are on a sideline (parallel to the engine

centerline) arc (see Fig. 5). Sound intensity flux through the cylindrical surface formed by the revolving the arc by 360^0 is therefore used as the sound power metric to compare predictions to measurements. Axisymmetric sound field is therefore assumed, which holds true when each tone has only one azimuthal (circumferential) mode. When multiple azimuthal modes are present, constructive and destructive interference in the azimuthal direction determines the azimuthal directivity. This assumption however should be true for most of the tones under consideration if the model is at perfectly zero angle of attack. One of the tones for a 12x10 configuration, for example, that will have multiple azimuthal modes is the tone at frequency 70Ω (Ω being the shaft rotation rate) as it arises from the combination (sum) of 5^{th} harmonic of the front rotor with the 1^{st} harmonic of the aft rotor ($(5\times12+1\times10)\Omega$) as well as the 7^{th} harmonic ($7 \times 10\Omega$) of the aft rotor.

Furthermore, the sound power radiated at very shallow angles, not covered by the microphones in the experiments, is ignored in the comparisons.

3. Results

Results from a recent test campaign [27, 23] conducted at the NASA 9'x15' low speed wind tunnel (LSWT) are used to verify the accuracy of the proposed prediction process. Elliott [27] describes in detail the LSWT test facility, the open rotor propulsion rig (ORPR), as well as the procedure for gathering far-field acoustic data in this facility. One of the many configurations tested in this campaign was designated as the F31A31 historical baseline

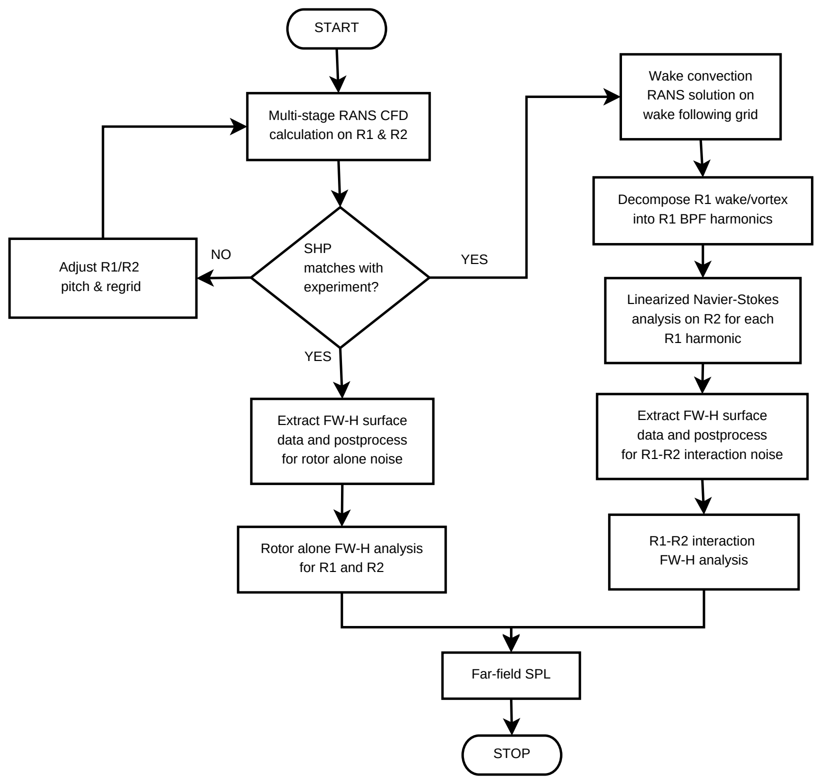

Figure 2: Flowchart of the open rotor noise prediction process.

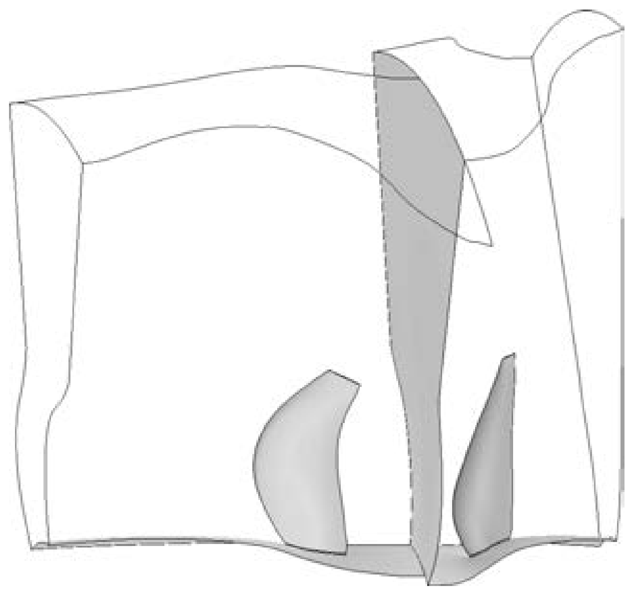

Figure 3: Multi-stage analysis configuration showing one blade each of the two bladerows of the F31A31 design and the interface plane. The front bladerow is referred to as R_1 and the aft, R_2.

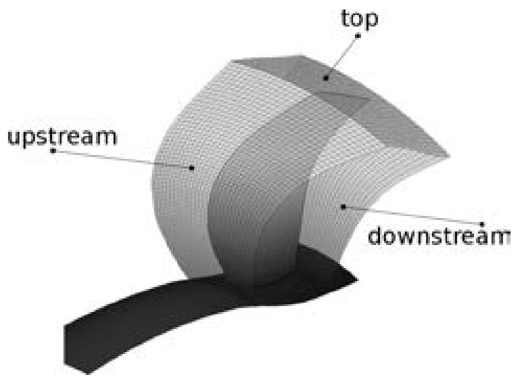

(a) Surfaces around one blade

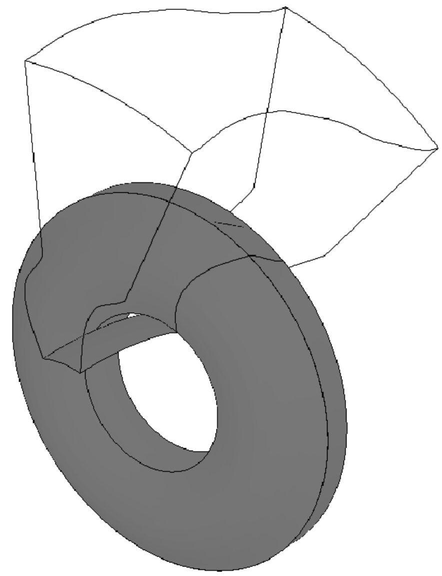

(b) Full-annulus FW-H surface

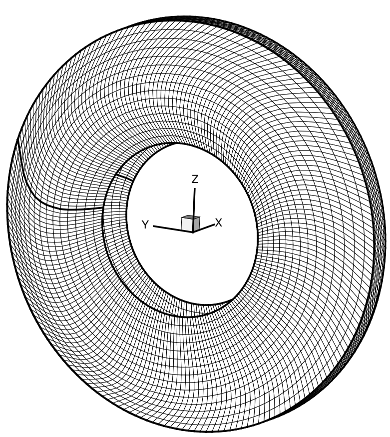

(c) Grid on FW-H surface

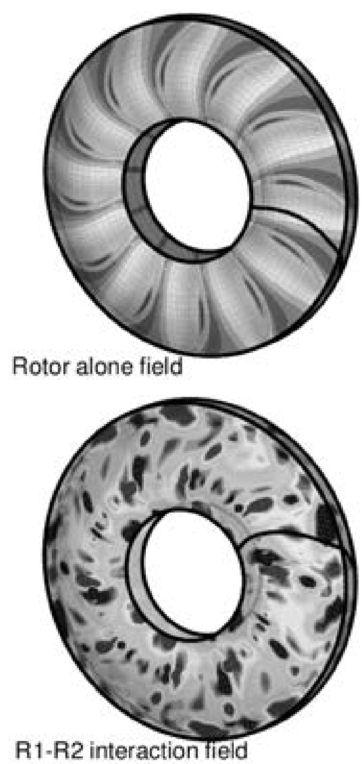

(d) Pressure contours

Figure 4: A description of the process of creating the FW-H surface: (a) surfaces in front (upstream), aft (downstream), and on top of (top) a single blade, (b) single passage to full annulus extension, (c) grid on the full FW-H surface, and (d) pressure contours on the FW-H surface for rotor alone and interaction noise computation. The two plots in (d) are on different scales.

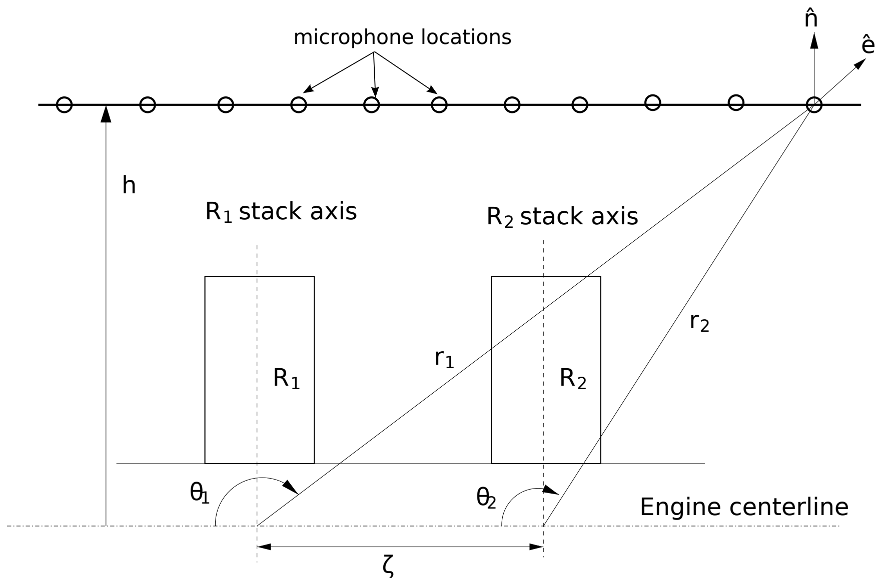

Figure 5: Schematic illustrating the sideline microphone locations.

design. This geometry has a 12-bladed front rotor and a 10-bladed aft rotor. Around the speed/thrust of interest (takeoff condition), the interaction tones dominate over the rotor-alone tones (arising from finite blade thickness and steady loading) and hence the focus here is on comparing interaction tones between data and predictions.

3.1. Ffowcs Williams-Hawkings Equation Solver

The Ffowcs Williams-Hawkings (FW-H) equation is a re-formulation of the linearized Euler equations using the Lighthill's acoustic analogy. A frequency domain formulation[6] of the FW-H equation is used here and the equations are provided in Appendix A.

A frequency domain FW-H equation solver is developed and validated against analytical solutions for point sources (monopole, dipole, and quadrupole) in a quiescent medium. A cube is defined around the point source at which the complete flow-field (density, pressure, and velocities) due to the source are computed analytically. The information on the six faces of the cube is then used by the FW-H solver to compute the sound pressure outside of the cube. Far-field directivities are compared for the three sources in Fig. 6, where excellent agreement can be observed.

Predictions are also made in the near field of the source, although it should be borne in mind that the derivation of the FW-H equation itself makes the approximation that the observer is in the far field. Hence the near-field solution cannot be expected to be exact. Comparisons are nevertheless made (see Fig. 7) in the near field as well, and are found to be reasonable except very near the surface. In Fig. 7, the nearest surface point is located at a distance of 2.12 units from the origin (shown by the arrow in the figure). The near field of the dipole and the quadrupole source is reasonably well captured, while the far-field prediction is excellent.

Since the interest is in predicting open rotor noise in flight condition (non-zero forward velocity), the FW-H code is also verified against the analytical solution of a point source in a moving medium. Three different flight speeds are considered, namely, flow Mach number equal to 0.25, 0.5, and 0.75. This adequately covers the range of flight speeds of interest although the focus of this paper is on noise during take-off, when the flight Mach number is around 0.25. Directivity comparisons in the far-field showing excellent agreement are plotted in Fig. 8.

These canonical validation cases provide sufficient confidence in the accuracy of the FW-H solver to attempt the open rotor noise prediction.

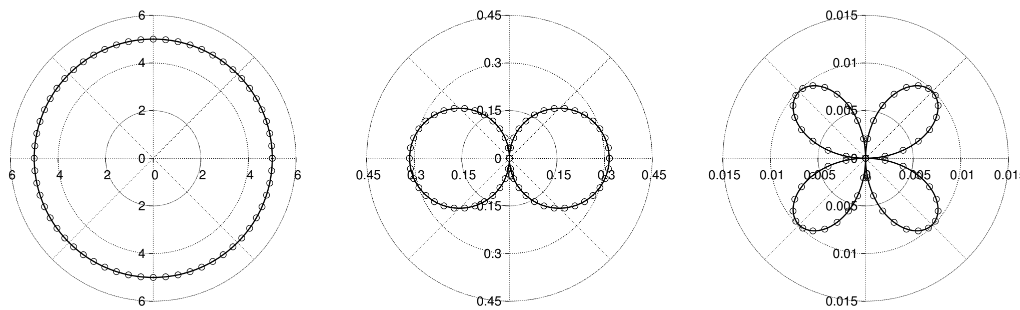

(a) Monopole (b) Dipole (c) Quadrupole

Figure 6: Directivity comparisons of pressure amplitude for a point source radiating in a quiescent medium between analytical solution (solid lines) and FW-H predictions (open circles). Pressure amplitudes are plotted in this polar plot.

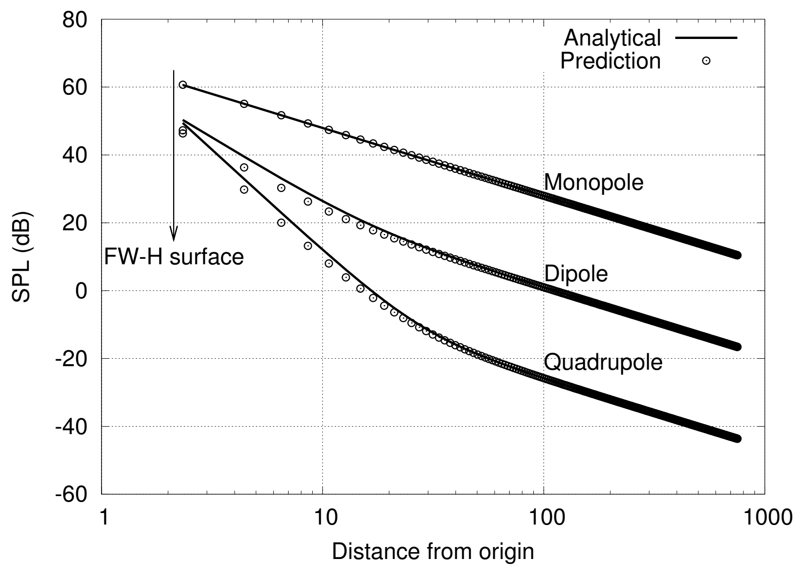

Figure 7: Near- and far-field comparisons of sound pressure levels (SPLs) between analytical solutions (solid lines) and FW-H predictions (open circles).

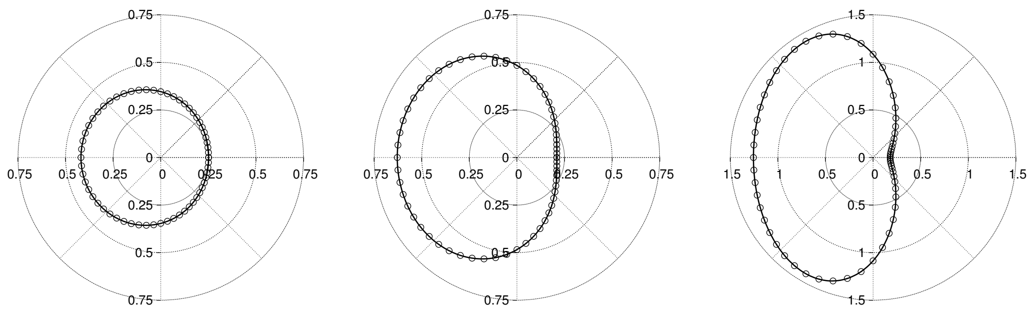

(a) M=0.25 (b) M=0.50 (c) M=0.75

Figure 8: Directivity comparisons of pressure amplitudes for a point source radiating in a moving medium between analytical solution (solid lines) and FW-H predictions (open circles). The axial flow Mach numbers considered are: (a) $M = 0.25$, (b) $M = 0.50$, and (c) $M = 0.75$.

3.2. Validation Against Test Data

For comparisons against test data, we focus our attention on the F31A31 geometry, a 12×10 configuration. The present investigation is further limited to studying the variation of noise with blade tip speed (RPM), while keeping the blade stagger angle fixed - the engine thrust is therefore not held constant. A number of changes occur with increasing rotational speed that all contribute to noise increase in an open rotor. These are - (1) increase in radiation efficiencies of the acoustic modes, (2) increase in rotor blade wake deficit (due to increased blade incidence), and (3) increased unsteady lift on the aft rotor due to (a) high relative velocity, and (b) high mean loading. The scaling with Mach number of different tones is determined by which of these dominate.

The proposed procedure for open rotor noise prediction does remarkably well in predicting the speed scaling of the rotor-rotor interaction tones, as is evident from Figs. 9 and 10, even though the absolute noise levels are slightly over-predicted. Linear curve fits (on a log-log scale) are plotted in the figures. The following nomenclature is used to represent the tones: $[a, b]$ refers to the tone at frequency $a\times$R1 BPF + $b\times$R2 BPF. In the cases considered here, both rotors (R1 and R2) rotate at the same shaft rotation rate, Ω. The sum tone $[a, b]$ therefore has a frequency of $(a\times\mathrm{N1} + b\times\mathrm{N2})\Omega$, where N1 and N2 are R1 and R2 blade counts respectively. Appendix B provides a mathematical reasoning for why the "sum" and "difference" tones appear in such interactions and shows the relationship between the interaction tone frequency and its azimuthal mode number.

Figure 9 compares the overall tone power level variation with blade speed between prediction and data, which is obtained by adding (log sum) the acoustic power in the dominant tones. The frequency domain analyses is carried out for the first four harmonics of R1, which implies that the simulations (theoretically) should predict the following tones: $[1, (1 \ldots \infty)]$, $[2, (1 \ldots \infty)]$, $[3, (1 \ldots \infty)]$ and $[4, (1 \ldots \infty)]$. Since the geometric resolution (mesh) of the aft rotor is finite, only a finite number of "scattered" modes can be captured in the linearized runs. Finite spatial order accuracy and artificial dissipation in the numerical scheme determine the grid resolution (number of points per wavelength) required to accurately resolve the higher order spatial modes. Only the first four scattered modes are therefore retained in the post-processing and used to compute the overall tonal power level. Similar filtering is applied to the experimental data as well to make a one-to-one comparison.

Figure 10 shows the speed trend comparison for four groups of tones.

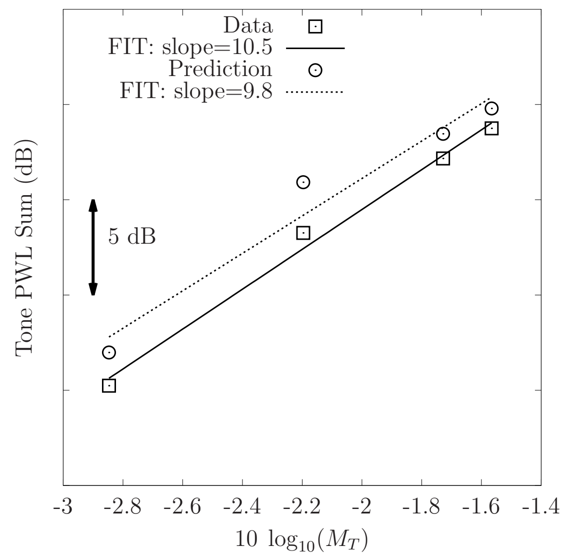

Figure 9: Comparison of measured and predicted sound power level sum of the rotor-rotor interaction tones.

These are grouped based on the wake harmonic of the front rotor. For example, in the figure, $(1, \sum_1^4)$ refers to the sum of $[1,1], [1,2], [1,3]$ & $[1,4]$ tones. Analyzing the results in such groups is useful as it identifies the contribution of noise by a specific wake harmonic of the front rotor. Good agreement is observed for these sets of comparisons as well. It is also noted that the overall tone power level (in Fig. 9) is very much governed by the interaction of the first wake/vortex harmonic of R1 with R2 (i.e., by the $[1, \sum_1^4]$ tones). While this is true for the cases considered here, it may not always hold true (e.g., at other blade pitch and speed settings).

Figure 11 compares the acoustic power in each tone between data and prediction. The agreement in general is good; the largest discrepancy is observed for tones with two properties: first, they are relatively low in noise

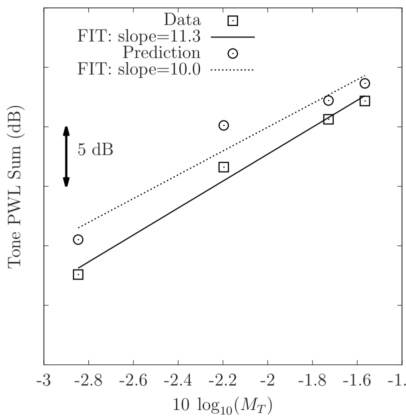

(a) $(1,\sum_1^4)$ tone sum

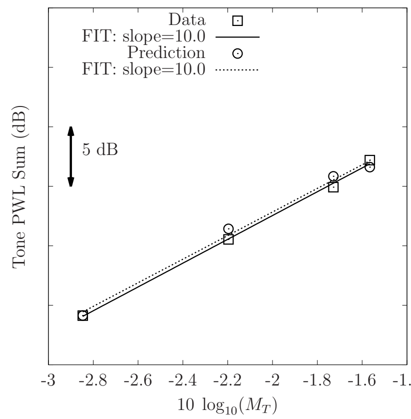

(b) $(2,\sum_1^4)$ tone sum

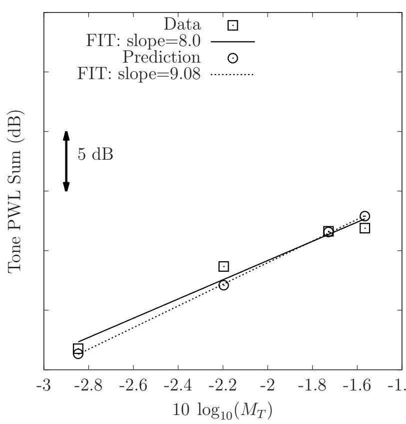

(c) $(3,\sum_1^4)$ tone sum

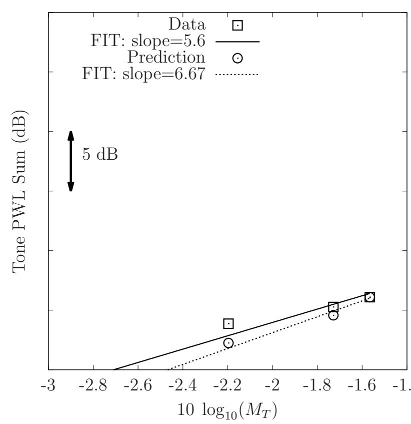

(d) $(4,\sum_1^4)$ tone sum

Figure 10: Comparison of measured and predicted sound power level sum grouped as blade passing harmonics of the front rotor.

amplitude (and hence less relevant to the overall tone noise level), and second, these tones should have a large azimuthal mode number if rotor-rotor interaction is the sole noise generation mechanism. As an example, consider the $[4, 1]$ tone. The predicted tone power level is more that 20 dB lower than measured data. The frequency of this tone is $(4 \times 12 + 1 \times 10)\Omega = 58\Omega$ while its circumferential mode number is $(4 \times 12 - 1 \times 10) = 38$. The radiation efficiency of this mode is very low as explained below. Radiation efficiency of each tone is given by a Bessel function of order equal to the azimuthal mode number and the argument given by the radial wave number multiplied by radius. The radial wave number is proportional to the frequency of the tone. Asymptotic behaviour of Bessel functions (as the argument becomes smaller than the order) is given by

$$J_n(x) \sim \frac{1}{n!} \left(\frac{x}{2} \right)^n \tag{1}$$

For relatively small speeds (Ω) considered here, the frequencies and hence the argument of the Bessel function becomes smaller than the order for a few tones (e.g., $[3, 1]$, $[4, 1]$, and $[4, 2]$) and hence their radiation efficiency plummets. Radiation efficiency of acoustic modes can also be explained using the concept of "sonic" or "Mach" radius introduced by Parry [28]. For a given observer location, the sonic radius is defined as the radius at which the source moves towards the observer at sonic speed. The sonic radius determines the dominant noise producing region. For modes where the argument of the Bessel function is smaller than the order (i.e., where Eq. 1 holds), the sonic radius lies outboard of the tip radius. These modes therefore have poor radiation efficiencies. This is further illustrated in Fig. 12 where far-field noise from a point source (as calculated using Hanson's noise radiation

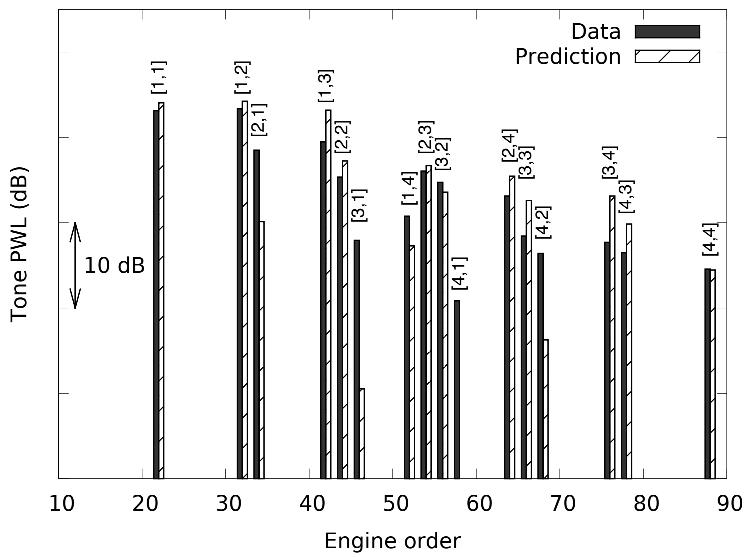

Figure 11: Interaction tone PWL spectra comparison between data and prediction at one sample operating point.

formula [11]) for different interaction tones are compared. Figure 12 demonstrates the variation of radiation efficiency with azimuthal mode number for a few tones. Plots (a) and (b) in Fig. 12 show the directivity of sets of tones $[1,1]$, $[1,2]$, $[1,3]$, $[1,4]$ and $[4,1]$, $[4,2]$, $[4,3]$, $[4,4]$ respectively. The reader is reminded that the azimuthal mode number of each tone is unique (theoretically) and is given by $(a \times N1 - b \times N2)$ for the tone $[a,b]$. The azimuthal mode numbers for these tones are also listed in parentheses in plots (c) and (d) of Fig. 12, which integrate the directivity and show the sound power levels (relative to the power in $[1,1]$ tone). As the azimuthal mode order increases, the sound radiation starts to concentrate in the plane of rotation and the radiation patters looks much like that of rotor alone noise (see e.g. directivity of $[4,1]$ tone in plot (b)). Integrated sound power levels confirm that increasing azimuthal mode order leads to drop in the sound power. Since the source amplitude in this canonical example is unity for all tones, the reduction in power is completely due to the reduction in radiation efficiency.

The predicted reduced levels of noise for tones $[3, 1]$, $[4, 1]$, and $[4, 2]$ in Fig. 11 therefore are expected due to the reduced radiation efficiencies of these modes. The relatively large power in the measured data for these tones may be explained by the following. It is conjectured that the origin of these tones in experiment is not simply due to R1-R2 interaction but perhaps due to the interaction of a "spatially modulated" R1 wake with R2. Such a modulation occurring for example if the open rotor operates at a slightly non-zero angle of attack. The interaction of such spatially modulated wake would then produce the same time spectral content but the azimuthal order of the modes would be lower, enhancing the radiation efficiency of these tones. In such cases, the directivity of the tones would show a variation with azimuthal angle. The current test campaign however did not include azimuthal directivity measurements, and hence it is not possibly to verify this hypothesis.

Another evidence of "unsuspected" noise radiation in the open rotor experiments is observed (see Fig. 13) in the spectral decay of rotor alone tones, e.g., consider R1 alone tones: $[n, 0]$, where $n = 12, 24, 36, \ldots$ etc. Analytical theories e.g., due to Gutin [29] as well as the predictions made herein suggest a sharp dropoff with higher harmonics of noise due to thickness and steady loading, due again to rapid reduction in radiation efficiency (through increase in the order of the Bessel function). Similar results (not shown here) were ob-

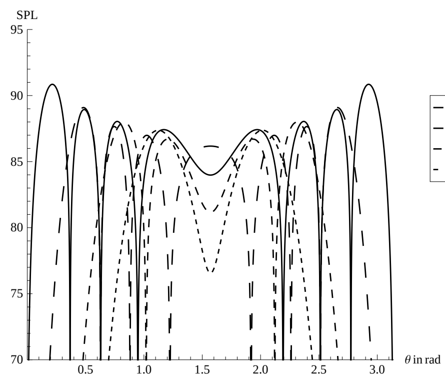

(a) Directivity of tones: (1,1. . .4)

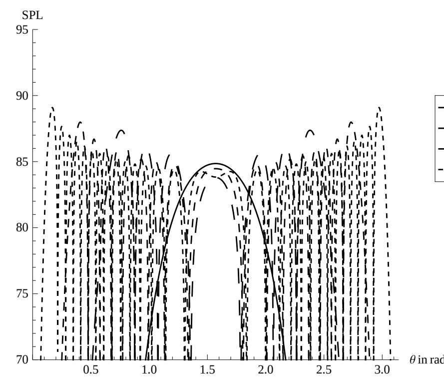

(b) Directivity of tones: (4,1. . .4)

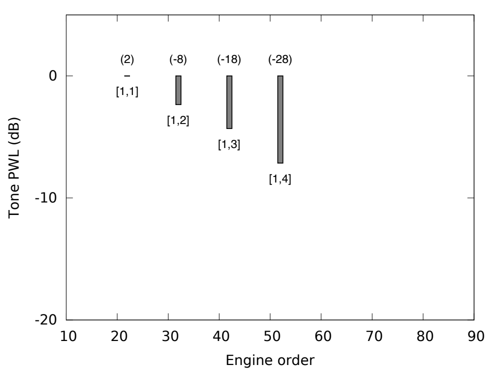

(c) PWL of tones: (1,1. . .4)

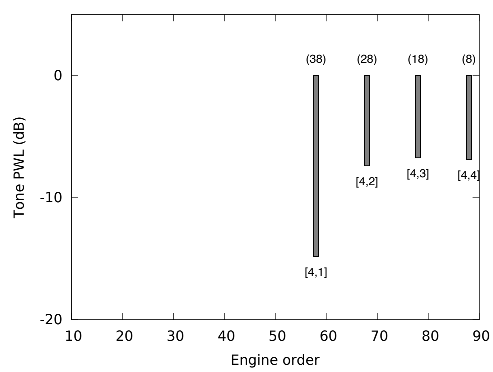

(d) PWL of tones: (4,1. . .4)

Figure 12: Directivity and sound power levels of selected interaction tones and for a model point source problem. Sound power is normalized so that $[1, 1]$ tone has PWL=0. In (c) and (d) the number in parentheses is the azimuthal mode order of the tone.

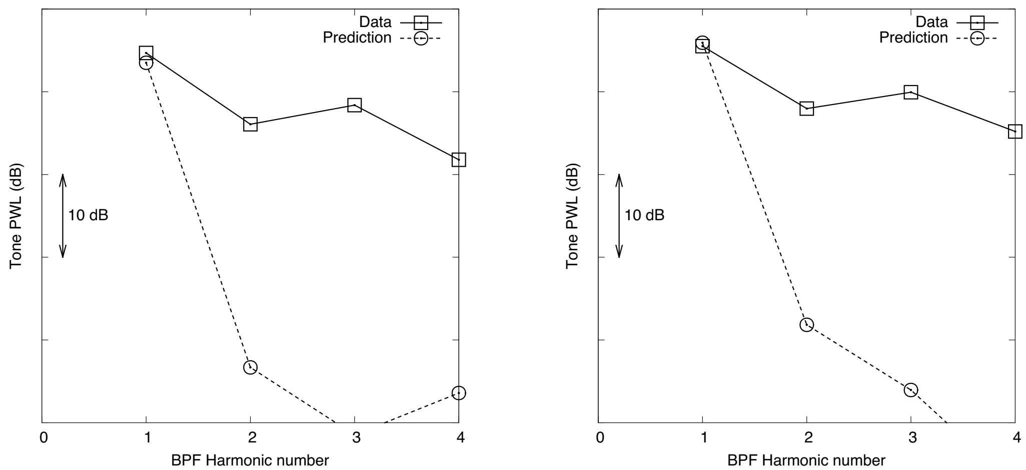

(a) R1 (b) R2

Figure 13: Variation of rotor alone acoustic power with (a) R1 and (b) R2 harmonics.

served with other semi-analytical prediction methods [30, 31]. Measured data shows some reduction but it is not as large and also it plateaus out around the second blade passing frequency. Note that this level is still above the measured broadband noise. Again, it is suspected that the measured noise here is due to a different source, e.g., inlet distortion. While there are turbulence screens employed in the experiment to minimize the inlet turbulence levels, there is still a possibility of having coherent turbulence structures chopped by the blades to produce tones at blade passing frequency. The azimuthal order of the pattern due to the interaction of these distortions with the rotor bladerows may be much lower than that for steady loading (thickness) noise source, making them highly efficient at radiating. It is suspected that noise due to such interaction masquerades as "rotor alone" tones especially at high frequencies.

4. Conclusion

A new prediction methodology utilizing linearized RANS analysis in combination with an integral method approach (Ffowcs Williams-Hawkings equation solution) to predict aerodynamic tonal noise from open rotors is presented. A frequency domain FW-H solver is developed and validated against analytical solutions of point sources (mono-, di-, and quadru-pole) in a quiescent medium as well as for a point monopole in a moving medium. The prediction process is then applied to the historic F31A31 open rotor baseline geometry recently tested at the NASA 9' x 15' low-speed wind tunnel. Noise trends with blade tip Mach number are compared to show the validity of the proposed prediction process. Very good agreement between prediction and data is observed in noise trends with blade tip speed. Absolute levels are slightly over-predicted (around 2-4 dB). Greatest mismatch between data and prediction (data being higher) is observed for tones which are expected to have very high circumferential mode number and therefore very low radiation efficiency. It is conjectured that the high acoustic power levels measured in such modes arise from "non-ideal" R1-R2 interaction such as would occur if the R1 wake is spatially modulated.

5. Acknowledgment

The authors would like to thank their GE Aviation colleagues Dr. John Wojno and Dr. Muni Majjigi for providing critical technical guidance in the execution of this project, and for their permission to publish this work. Thanks are also due to NASA Glenn for test execution and for providing the data for comparison. Contributions from GE-GRC colleagues - Drs.

Chingwei Shieh, Trevor Wood, Kishore Ramakrishnan, Lawrence Cheung, and Umesh Paliath in improving the prediction quality are also recognized. Thanks are also due to Dr. Ramani Mani who provided very valuable input on the validation test cases.

Appendix A. FW-H Formulation

The permeable surface Ffowcs Williams-Hawkings equation, upon ignoring the volume integral term, can be written as

$$4\pi\,|\mathbf{x}|\,p'(\mathbf{x},t) = \frac{x_i}{c\,|\mathbf{x}|}\frac{\partial}{\partial t}\int\left[p'n_i + \rho u_i(u_j - U_j)n_j\right]\,\mathrm{d}\Sigma + \frac{\partial}{\partial t}\int\left[\rho_0 u_i + \rho'(u_i - U_i)\right]n_i\,\mathrm{d}\Sigma, \tag{A.1}$$

where Σ denotes the surface enclosing all the sound sources for the given problem. The sound emitted by the source located at $\mathbf{x_s}$ at time τ is received by the observer located at $\mathbf{x}$ at time t. The relation between the source time, τ and the observer time, t is

$$c(t-\tau) = |\mathbf{x} - \mathbf{x_s}|\,, \tag{A.2}$$

where c is the speed of sound. For an observer in the farfield ($|\mathbf{x}| \gg |\mathbf{x_s}|$) Eq. A.2 can be approximated as

$$c(t-\tau) \approx |\mathbf{x}| - \frac{\mathbf{x_s}.\mathbf{x}}{|\mathbf{x}|}. \tag{A.3}$$

Recognizing that the source $\mathbf{x_s}$ is located at $\mathbf{x_s} = \mathbf{y}$ at time $\tau = 0$ and moves with the velocity $\mathbf{U}$ (i.e., $\mathbf{x_s} = \mathbf{y} + \mathbf{U}\tau$), Eq. A.3 can be further expanded as

$$
\begin{aligned}
c(t-\tau) &\approx |\mathbf{x}| - \frac{\mathbf{x}.\mathbf{y}}{|\mathbf{x}|} - \frac{\tau\mathbf{U}.\mathbf{x}}{|\mathbf{x}|}, \text{ or,} \\
t-\tau &\approx \frac{|\mathbf{x}|}{c} - \frac{\mathbf{x}.\mathbf{y}}{c\,|\mathbf{x}|} - \frac{\tau\mathbf{U}.\mathbf{x}}{c\,|\mathbf{x}|}, \text{ or,} \\
(1-M_r)\tau &\approx t - \frac{|\mathbf{x}|}{c} + \frac{\mathbf{x}.\mathbf{y}}{c\,|\mathbf{x}|}.
\end{aligned} \tag{A.4}
$$

where M_r is the source Mach number in the direction of the observer. Taking the derivative of Eq. A.4 w.r.t. τ gives

$$
\begin{aligned}
(1-M_r)\frac{\mathrm{d}\tau}{\mathrm{d}t} &= 1, \text{ or,} \\
\frac{\mathrm{d}\tau}{\mathrm{d}t} &= \frac{1}{1-M_r},
\end{aligned} \tag{A.5}
$$

which is the Doppler frequency shift. The source angular frequency, ω is perceived by the observer to be $\omega/(1-M_r)$. Fourier transform Eq. A.1 to write the observer sound pressure at the frequency, $\omega/(1-M_r)$ as

$$
\begin{aligned}
4\pi\,|\mathbf{x}| \int_{-\infty}^{\infty} p'(\mathbf{x},t) e^{-\frac{i\omega t}{1-M_r}}\ \mathrm{d}t &= \frac{x_i}{c\,|\mathbf{x}|} \int_{-\infty}^{\infty} \left\{ \frac{\partial}{\partial t} \int \left[p' n_i + \rho u_i (u_j - U_j) n_j\right]\ \mathrm{d}\Sigma \right\} e^{-\frac{i\omega t}{1-M_r}}\ \mathrm{d}t \\
&+ \int_{-\infty}^{\infty} \left\{ \frac{\partial}{\partial t} \int \left[\rho_0 u_i + \rho'(u_i - U_i)\right] n_i\ \mathrm{d}\Sigma \right\} e^{-\frac{i\omega t}{1-M_r}}\ \mathrm{d}t.
\end{aligned} \tag{A.6}
$$

Convert $\dfrac{\partial}{\partial t} \to \dfrac{\partial}{\partial \tau}$ and $\mathrm{d}t \to \mathrm{d}\tau$ in the above using Eq. A.5 to get

$$
\begin{aligned}
4\pi\,|\mathbf{x}|\, \hat{p}(\mathbf{x}, \frac{\omega}{1-M_r}) &= \frac{x_i}{c(1-M_r)\,|\mathbf{x}|} \int_{-\infty}^{\infty} \left\{ \frac{\partial}{\partial \tau} \int \left[p' n_i + \rho u_i (u_j - U_j) n_j\right]\ \mathrm{d}\Sigma \right\} e^{-\frac{i\omega t}{1-M_r}}\ (1-M_r)\mathrm{d}\tau \\
&+ \frac{1}{(1-M_r)} \int_{-\infty}^{\infty} \left\{ \frac{\partial}{\partial \tau} \int \left[\rho_0 u_i + \rho'(u_i - U_i)\right] n_i\ \mathrm{d}\Sigma \right\} e^{-\frac{i\omega t}{1-M_r}}\ (1-M_r)\mathrm{d}\tau.
\end{aligned} \tag{A.7}
$$

The hat ($\hat{}$) denotes a Fourier transformed quantity. Using Eq. A.4 to express t in terms of the source time τ in the exponent gives

$$\begin{aligned} 4\pi\,|\mathbf{x}|\,\hat{p}(\mathbf{x},\frac{\omega}{1-M_r}) &= \frac{x_i}{c\,|\mathbf{x}|}\int\limits_{-\infty}^{\infty}\left\{\frac{\partial}{\partial\tau}\int\left[p'n_i+\rho u_i(u_j-U_j)n_j\right]\,\mathrm{d}\Sigma\right\}e^{-i\omega\tau}\mathrm{d}\tau e^{-\frac{i\omega}{1-M_r}\left(\frac{|\mathbf{x}|}{c}-\frac{\mathbf{x}.\mathbf{y}}{c|\mathbf{x}|}\right)} \\ &+ \int\limits_{-\infty}^{\infty}\left\{\frac{\partial}{\partial\tau}\int\left[\rho_0 u_i+\rho'(u_i-U_i)\right]n_i\,\mathrm{d}\Sigma\right\}e^{-i\omega\tau}\,\mathrm{d}\tau\;e^{-\frac{i\omega}{1-M_r}\left(\frac{|\mathbf{x}|}{c}-\frac{\mathbf{x}.\mathbf{y}}{c|\mathbf{x}|}\right)} \end{aligned} \tag{A.8}$$

The constant phase shift, $\exp\left(-\frac{i\omega}{1-M_r}\frac{|\mathbf{x}|}{c}\right)$, which represents the time delay for the sound to reach the observer, can be dropped from the above to write

$$\begin{aligned} 4\pi\,|\mathbf{x}|\,\hat{p}(\mathbf{x},\frac{\omega}{1-M_r}) &= \frac{x_i}{c\,|\mathbf{x}|}\int\limits_{-\infty}^{\infty}\left\{\frac{\partial}{\partial\tau}\int\left[p'n_i+\rho u_i(u_j-U_j)n_j\right]\,\mathrm{d}\Sigma\right\}e^{-i\omega\tau}\mathrm{d}\tau e^{-\frac{i\omega}{1-M_r}\left(-\frac{\mathbf{x}.\mathbf{y}}{c|\mathbf{x}|}\right)} \\ &+ \int\limits_{-\infty}^{\infty}\left\{\frac{\partial}{\partial\tau}\int\left[\rho_0 u_i+\rho'(u_i-U_i)\right]n_i\,\mathrm{d}\Sigma\right\}e^{-i\omega\tau}\,\mathrm{d}\tau\;e^{-\frac{i\omega}{1-M_r}\left(-\frac{\mathbf{x}.\mathbf{y}}{c|\mathbf{x}|}\right)} \end{aligned} \tag{A.9}$$

The partial derivative operator, $\partial/\partial\tau$ can be taken inside the Σ integral as it is independent of τ. Further, realizing that

$$\int\limits_{-\infty}^{\infty}\frac{\partial\psi(\tau)}{\partial\tau}\exp\left(-i\omega\tau\right)\mathrm{d}\tau = i\,\omega\int\limits_{-\infty}^{\infty}\psi(\tau)\exp\left(-i\omega\tau\right)\mathrm{d}\tau, \tag{A.10}$$

Eq. A.9 can be rewritten as

$$\begin{aligned} 4\pi\,|\mathbf{x}|\,\hat{p}(\mathbf{x},\frac{\omega}{1-M_r}) &= i\omega\frac{x_i}{c\,|\mathbf{x}|}\int\left[p'n_i+\rho\widehat{u_i(u_j}-U_j)n_j\right]\,\exp\left\{-\frac{i\omega}{1-M_r}\left(-\frac{\mathbf{x}.\mathbf{y}}{c\,|\mathbf{x}|}\right)\right\}\mathrm{d}\Sigma \\ &+ i\omega\int\left[(\rho_0 u_i+\widehat{\rho'(u_i}-U_i))n_i\right]\,\exp\left\{-\frac{i\omega}{1-M_r}\left(-\frac{\mathbf{x}.\mathbf{y}}{c\,|\mathbf{x}|}\right)\right\}\mathrm{d}\Sigma \end{aligned} \tag{A.11}$$

which is the form of the integral equation used here.

Appendix B. R1-R2 Interaction Noise

A mathematical reasoning for the generation of sum and difference tones due to rotor-rotor (R1-R2) interaction is given below. In the stationary, cylindrical frame of reference (x, r, θ, t), the R1 wake can be represented by

$$V_g = \sum_{n=0}^{\infty} \hat{V}_g(x, r) \exp\left\{i\ n\ N_{R_1}(-\Omega_1 t + \theta)\right\}, \tag{B.1}$$

where Ω_1 is the angular velocity of R1. In the frame of reference attached to R2, (x', r', θ', t') where

$$x' = x, r' = r, t' = t,\ \&\ \theta' = \theta + \Omega_2 t,$$

the wake/gust appears as

$$V_g = \sum_{n=0}^{\infty} \hat{V}_g(x', r') \exp\left\{i\ n\ N_{R_1}(-(\Omega_1 + \Omega_2)t + \theta')\right\}. \tag{B.2}$$

Hence, the frequency of the gust in the R2 frame of reference is $\omega'_g = nN_{R_1}(\Omega_1 + \Omega_2)$. This is the frequency at which the forced response calculation using linearized RANS is carried out. The solution of the linearized RANS equations yields near-field pressure in the R2 frame of reference, which can be written as

$$p = \sum_{n=0}^{\infty} \sum_{k=-\infty}^{\infty} \hat{p}(x', r') \exp\left\{i(-\omega t + m'\theta')\right\}, \tag{B.3}$$

where $m' = nN_{R_1} - kN_{R_2}$ and k is an integer, as given by the Tyler-Sofrin theory [32]. Writing the above expression in the ground frame of reference gives

$$\begin{aligned} p &= \sum_{n=0}^{\infty} \sum_{k=-\infty}^{\infty} \hat{p}(x', r') \exp\left\{i(-nN_{R_1}(\Omega_1 + \Omega_2)t + (nN_{R_1} - kN_{R_2})(\theta + \Omega_2 t))\right\} \\ &= \sum_{n=0}^{\infty} \sum_{k=-\infty}^{\infty} \hat{p}(x, r) \exp\left\{i(-(nN_{R1}\Omega_1 + kN_{R_2}\Omega_2)t + (nN_{R_1} - kN_{R_2})\theta)\right\} \end{aligned} \tag{B.4}$$

Equation B.4 suggests that the frequencies of the R1-R2 interaction tones, and the corresponding circumferential modes are given by

$$\omega_p = (nN_{R_1}\Omega_1 + kN_{R_2}\Omega_2) \text{ and } m = nN_{R_1} - kN_{R_2} \text{ respectively.}$$

Note that Ω_1 and Ω_2 are magnitudes of the shaft rotation rates; the direction of rotation is taken into account in relating θ' to θ. For the case when the shaft rotation rates of the two rotors are equal ($\Omega_1 = \Omega_2 = \Omega$), the expression for interaction frequencies reduces to

$$\omega_p = (nN_{R_1} + kN_{R_2})\Omega, \quad \text{where } -\infty < k < \infty,$$

and hence the expression "sum" and "difference" tones is used to refer to rotor-rotor interaction tones.

Note that while the "sum" tones are easily observed in experiments, the "difference" tones hardly are. This is primarily because the circumferential mode number corresponding to a "difference" tone is much higher (which corresponds to the order of the Bessel function) while the frequency (which corresponds to the argument of the Bessel function) is much lower, thus rendering the radiation efficiency of "difference" tones to be very low.

References

[1] A. B. Parry, M. Kingan, B. J. Tester, Relative importance of open rotor tone and broadband sources, in: Proceedings of the 17*th* AIAA/CEAS Aeroacoustics Conference (32*nd* AIAA Aeroacoustics Conference), Portland, OR.

[2] A. Sharma, S. K. Richards, T. H. Wood, C. M. Shieh, Numerical prediction of exhaust fan-tone noise from high-bypass aircraft engine, AIAA Journal 47 (2009).

[3] J. Verdon, Linearized unsteady aerodynamic analysis of the acoustic response of wake/blade-row interaction, NASA/CR–2001-210713 (2001).

[4] D. Prasad, J. M. Verdon, A three-dimensional linearized euler analysis of classical wake/stator interactions: Validation and unsteady response predictions, International Journal of Aeroacoustics 1 (2002) 137–163.

[5] J. E. Ffowcs Williams, D. L. Hawkings, Sound generated by turbulence and surfaces in arbitrary motion, Philosophical Transactions of the Royal Society A264 (1969) 321–342.

[6] M. L. Shur, P. R. Spalart, M. Strelets, Noise prediction for increasingly complex jets. part i: Methods and tests, International Journal of Aeroacoustics 4 (2005) 213–246.

[7] D. G. Holmes, B. E. Mitchell, C. B. Lorence, Three dimensional linearized navier-stokes calculations for flutter and forced response, in: Proceedings of the 8th ISUAAT Symposium, Stockholm, Sweden.

[8] M. Nyukhtikov, N. Smelova, B. E. Mitchell, D. G. Holmes, Optimized dual-time stepping technique for time-accurate navier-stokes calculations, in: Proceedings of the 14th ISUAAT Symposium, Duke University.

[9] N. Peake, A. B. Parry, Modern challenges facing turbomachinery aeroacoustics, Annual Review of Fluid Mechanics 44 (2012) 227–248.

[10] H. H. Hubbard, Sound from Dual-Rotating and Multiple Rotating Propellers, Technical Report, NACA TN 1654, 1948.

[11] D. B. Hanson, Noise of counter-rotation propellers, AIAA Journal of Aircraft 22 (1985) 609–617.

[12] D. B. Hanson, Compressible helicoidal surface theory for propeller aerodynamics and noise, AIAA Journal 21 (1983) 881–889.

[13] R. Mani, The radiation of sound from a propeller at angle of attack, Proceedings of the Royal Society A 431 (1990) 203–218.

[14] D. B. Hanson, Sound from a propeller at angle of attack: A new theoretical viewpoint, Proceedings of the Royal Society A 449 (1995) 315–328.

[15] A. Carazo, M. Roger, M. Omais, Analytical prediction of wake-interaction noise in counter-rotation open rotors, in: 17th AIAA/CEAS Aeroacoustics Conference, AIAA 2011-2758.

[16] V. P. Blandeau, P. F. Joseph, Broadband noise due to rotor-wake/rotor interaction in contra-rotating open rotors, AIAA Journal 11 (2010) 2674–2686.

[17] P. Spalart, Initial noise predictions for open rotors using first principles, in: AIAA Aeroacoustics Conference, AIAA-2010-3794, American Institute of Aeronautics and Astronautics, Stockholm, Sweden.

[18] A. Peters, Z. S. Spakovszky, Rotor interaction noise in counter-rotating propfan propulsion systems, Journal of Turbomachinery 134 (2012).

[19] T. Deconinck, A. Capron, C. Hirsch, G. Ghorbaniasl, Prediction of near- and far-field noise generated by contra-rotating open rotors, International Journal of Aeroacoustics 11 (2012) 219–238.

[20] Y. Colin, A. Carazo, B. Caruelle, T. Nodé-Langlois, Computational strategy for predicting cror noise at low-speed. part i: Review of numerical methods, in: 18th AIAA/CEAS Aeroacoustics Conference, AIAA 2012-2221, American Institute of Aeronautics and Astronautics, Colorado Springs, CO.

[21] Y. Colin, F. Blanc, B. Caruelle, F. Barrois, Computational strategy for predicting cror noise at low-speed. part ii: Investigation of the noise sources computation with the chorochronic approach, in: 18th AIAA/CEAS Aeroacoustics Conference, AIAA 2012-2222, American Institute of Aeronautics and Astronautics, Colorado Springs, CO.

[22] Y. Colin, B. Caruelle, Computational strategy for predicting cror noise at low-speed. part iii: Investigation of the noise radiation with the ffowcs williams-hawkings analogy, in: 18th AIAA/CEAS Aeroacoustics Conference, AIAA 2012-2223, American Institute of Aeronautics and Astronautics, Colorado Springs, CO.

[23] D. B. Stephens, E. Envia, Acoustic shielding for a model scale counter-rotation open rotor, in: Proceedings of the 17th AIAA/CEAS Aeroacoustics Conference, AIAA 2011-2940, Portland, Oregon.

[24] A. McAlpine, M. J. Kingan, Far-field sound radiation due to an installed open rotor, International Journal of Aeroacoustics 11 (2012) 213–245.

[25] M. Kingan, C. Powles, R. Self, Effect of centerbody scattering on advanced open-rotor noise effect of centerbody scattering on advanced open-rotor noise, AIAA Journal 48 (2010) 975–980.

[26] A. Sharma, H. Chen, C. M. Shieh, Linearized navier-stokes analysis for rotor-stator interaction tone noise prediction, in: 16th AIAA Aeroacoustics Conference, Paper 2010-3744, Stockholm, Sweden.

[27] D. M. Elliot, Initial investigation of the acoustics of a counter-rotating open rotor model with historical baseline blades in a low-speed wind tunnel, in: Proceedings of the 17th AIAA/CEAS Aeroacoustics Conference, AIAA 2011-2760, Portland, Oregon.

[28] A. B. Parry, Theoretical Prediction of Counter-Rotating Propeller Noise, Ph.D. thesis, University of Leeds, 1988.

[29] L. Gutin, On the Sound Field of a Rotating Propeller, Technical Report, NACA TM 1195, 1948.

[30] C. E. Whitfield, P. R. Gliebe, Predicted vs. scale model and flight test udfr engine noise, in: 13th AIAA Aeroacoustics Conference, Paper 90-3936, Tallahassee, Florida, USA.

[31] C. E. Whitfield, R. Mani, P. R. Gliebe, High speed turboprop aeroacoustic study, in: NASA Contractor Report 185241.

[32] J. M. Tyler, T. G. Sofrin, Axial flow compressor noise studies, SAE Transactions 70 (1962) 309–332.